JOURNAL OF GEOPHYSICAL RESEARCH, VOL. 104, NO. C6, PAGES 13,541–13,557, JUNE 15, 1999

Simulation of the semidiurnal tides in the Strait of Gibraltar

Luis Tejedor and Alfredo Izquierdo
Departamento de Física Aplicada, Universidad de Cádiz, Puerto Real (Cádiz), Spain

Boris A. Kagan and Dmitry V. Sein
P.P. Shirshov Institute of Oceanology, Russian Academy of Sciences, St. Petersburg

Abstract. The M_2 and S_2 surface tides in the Strait of Gibraltar are simulated using a two-dimensional, nonlinear, boundary-fitted coordinate model with a nominal resolution of ~0.5 km. Good agreement is achieved with tide gauge and bottom pressure observations, as well as with current measurements made during the Gibraltar Experiment. The cotidal charts and the maps of tidal current ellipse parameters, which have been constructed on the basis of the model results, reproduce all of the known features of the spatial structure of the M_2 and S_2 tidal waves. These results also show that a ~90° phase difference between tidal velocity and elevation is detected in much of the Strait of Gibraltar, thus suggesting a small mean tidal energy flux through the strait. The model results give evidence of the general direction for the M_2 and S_2 net tidal energy fluxes to the west. This finding is consistent with an observed southwestern tidal phase propagation and remains qualitatively unchanged when varying the strait's geometry as well as boundary and astronomical forcings.

1. Introduction

According to *Candela et al.* [1990], the most remarkable features of the semidiurnal surface tides in the Strait of Gibraltar are (1) a more than twofold decrease in amplitudes and slight variations in phases of the M_2 tidal wave along the strait, (2) a prevailing propagation of the phases southwestward, (3) a phase difference of almost 90° between the M_2 tidal velocity and elevation at the Camarinal Sill, and (4) rather constant amplitude ratios and phase differences between the M_2 and S_2 tidal constituents throughout the strait. *Candela et al.* [1990] explained some of these features using as a basis for interpretation the analytical model of *Rocha and Clarke* [1987] for tidal interaction between two oceans of constant depth joined by a narrow rectangular strait. This model, when applied to the Strait of Gibraltar, predicts a linear decrease in amplitudes from west to east and a southeast tidal phase propagation instead of the observed southwest propagation. Furthermore, since this model ignores the effect of topographic funnelling, it cannot provide an exhaustive explanation for the tidal dynamics in the strait. Thus the nature and energetics of the semidiurnal tides in the Strait of Gibraltar, as defined from analysis of experimental data, are still not completely understood.

The same may be said with respect to existing numerical models for the semidiurnal surface tides in the Strait of Gibraltar. At present, there are at least three of those models; namely, those of *Sánchez and Pascual* [1988], *Wang* [1989, 1993], and *González et al.* [1995]. The first of them is a two-dimensional (2-D) nonlinear, finite-difference model with prescribed values of tidal elevation at open boundaries and a grid spatial resolution of 2.5 km; the second is a 3-D, nonlinear, finite-difference model with a prescribed identical tidal transport at open boundaries and a grid spatial resolution of 4.6 km along latitude and 5.0 km along longitude; and the third is a 2-D, nonlinear, finite-element model with prescribed values of tidal elevation at open boundaries and a nominal spatial resolution of ~2.0 km. All the models reproduced a twofold decrease in amplitudes from the western to eastern end of the strait as well as small variations in phases within the strait and a ~90° phase difference between tidal velocity and elevation. However, the nature of these features remained unexplored. Moreover, the energetics of the semidiurnal surface tides in the Strait of Gibraltar were not discussed, and the model results were not sufficiently verified.

We have already mentioned topographic funnelling, which may be responsible for a nearly 90° phase difference between tidal velocity and elevation. This subject merits closer attention. Topographic funnelling (a term introduced by *Jay* [1991]) is defined as the direct dependence of tidal characteristics on the geometry of a channel. As was stated first by *Hunt* [1964] and thereafter by *Jay* [1991] and *Friedrichs and Aubrey* [1994], the nature of tidal waves in strongly convergent channels with friction is fundamentally different from that of classical damped tidal co-oscillations. This means that in a channel of uniform width and depth, an incident wave produces a 90° phase difference between tidal velocity and elevation only when it interacts with a reflected wave of nearly equal amplitude, in contrast to a channel with an exponential change in cross-sectional area, where the same incident wave can produce an identical phase difference without the presence of a reflected wave.

Jay [1991] analyzed the asymptotic cases of weak convergence (friction and changes in geometry are weak relative to the acceleration), strong convergence (friction and acceleration are weak relative to the effect of geometry), critical convergence (acceleration and geometry effects are equal and of opposite sign), and supercritical convergence (strong changes in geometry with weak friction). He showed that the phase difference in exponentially convergent channels was ~0° just

Paper number 1998JC900102.
0148-0227/99/1998JC900102$09.00

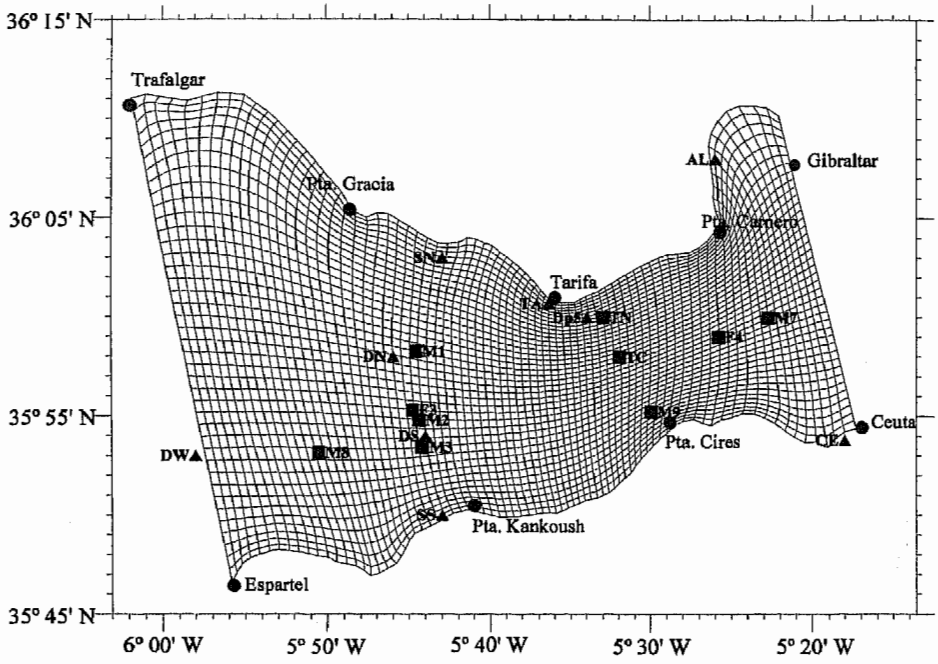

Figure 1. Grid map of the Strait of Gibraltar. Also shown are the locations of the bottom pressure (solid triangles), tide gauge (solid circles) and current velocities (solid rectangles) measurements referred to in the text.

below critical convergence and ~90° just above, with a rather abrupt change in critical convergence.

Another asymptotic case of strong convergence with strong friction was examined in detail by *Friedrichs and Aubrey* [1994]. They found from a scaling of the governing equations describing tidal propagation in a shallow channel with exponentially changing width and cross-sectional area that at lowest order, along-channel gradients in cross-sectional area override associated gradients in velocity in the continuity equation, and friction overrides acceleration in the momentum equation. Accordingly, the initial equations are reduced to the first-order wave equation describing a unidirectional wave. This wave exhibits properties of both progressive and standing waves simultaneously. That is, like a progressive wave, it has a constant amplitude and a phase speed near its inviscid value. On the other hand, as for a standing wave, the phase difference between tidal velocity and elevation is ~90°.

The paper is organized as follows. Section 2 contains a brief description of a 2-D, high-resolution, nonlinear, boundary-fitted coordinate model applied to the simulation of the M_2 and S_2 surface tides in the Strait of Gibraltar. In section 3 the results are compared with coastal tide gauge and bottom pressure observational data as well as with available data of current measurements made during the Gibraltar Experiment. The analysis of the spatial structure and energetics of the semidiurnal surface tides is also presented. Then the results of the sensitivity studies with regard to boundary and astronomical forcings and changing geometry, as well as the significance of the end and topographic funnelling effects, are discussed in section 4. The conclusions are drawn in section 5, followed by Appendix A, where the model equations, boundary conditions, and information on the method of solution are presented. Finally, in Appendix B, the lowest-order solution to a simple model problem is given, illustrating the effect of topographic funnelling on tidal propagation in a weakly dissipative, narrow channel with small variation in geometry and the topographic length scale being much smaller than a characteristic tidal wavelength.

2. Model Description

The numerical model for simulating the semidiurnal surface tides in the Strait of Gibraltar is a 2-D, high-resolution, nonlinear, boundary-fitted coordinate model. A brief description of the model is given in Appendix A. The following boundary conditions are used. A free-slip condition for velocity is applied at the coastal boundaries. At the open boundaries, the boundary conditions specified there should be chosen such that the boundary value problem is well posed. It is known that the boundary value problem of the quasi-hyperbolic type for the shallow-water equations is well posed if two boundary conditions are set at the inflow points of the open boundaries. The form of these conditions has been analyzed by *Oliger and Sandstrom* [1978], who showed that one of the boundary conditions should be of the form of an impedance relation between the contravariant component of tidal velocity and elevation. As an additional condition at the inflow points, a contravariant component of velocity should be specified. The required information at the open boundaries is, however, usually lacking, and the above conditions are replaced by simplified ones, with the tidal elevation being prescribed as a periodic function of time. Following standard practice, we shall also employ this condition at the open boundaries of the strait. In the present formulation, this is equivalent to the assignment of a certain cut-off function which eliminates the advective transport of momentum in the immediate vicinity of these boundaries. According to *Androsov et al.* [1995], the difference between the two solutions corresponding to the exact and simplified boundary conditions becomes smaller with increasing depth.

The curvilinear grid with a nominal spatial resolution of 0.5

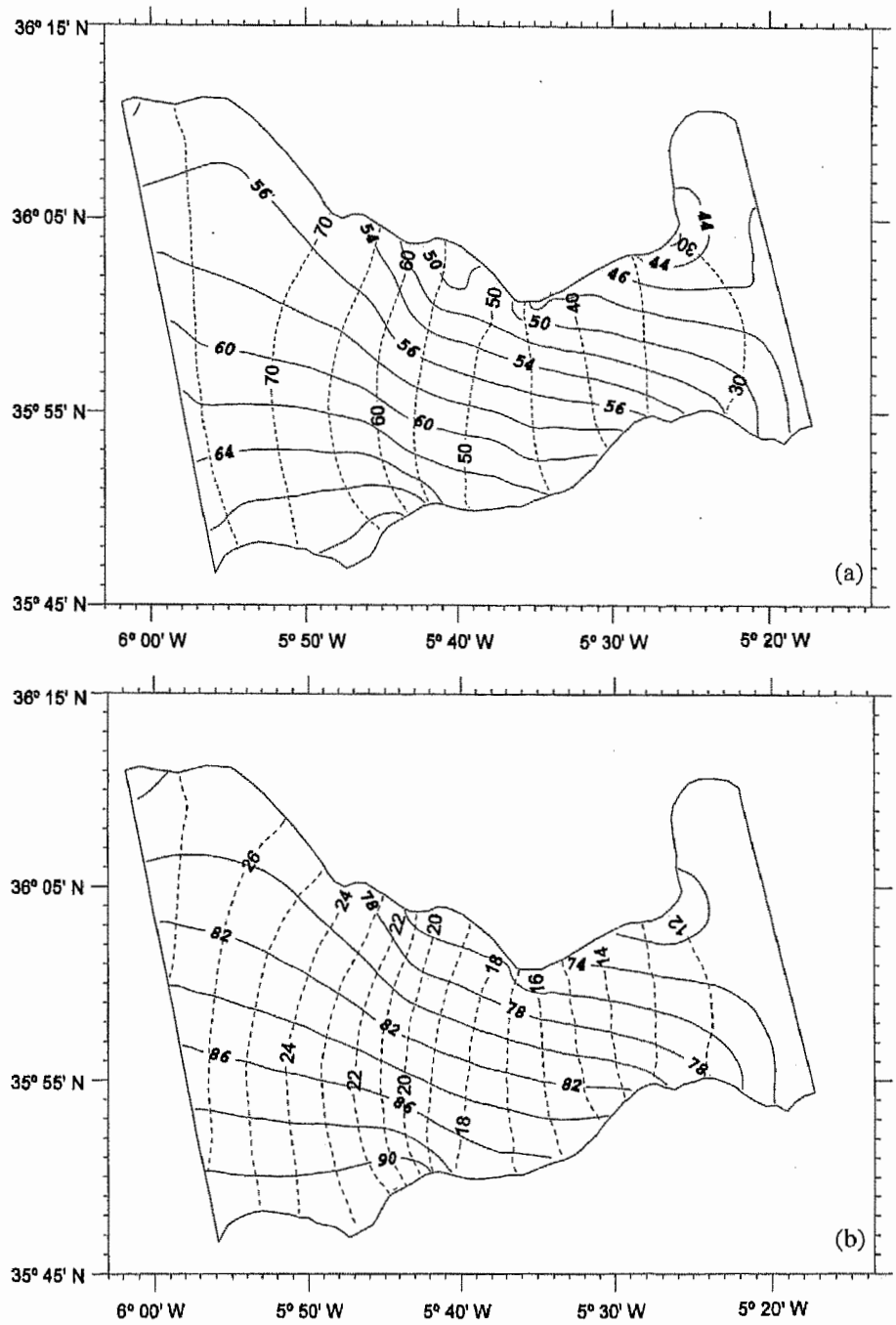

Figure 2. Cotidal charts of the (a) M_2 and (b) S_2 surface tides. Solid lines are phase contours, in degrees; dashed lines are amplitude contours, in centimeters.

km is displayed in Figure 1. The tidal constants at the open boundary grid nodes were obtained by interpolating between those at Trafalgar and Espartel on the western end, and Gibraltar and Ceuta on the eastern end of the strait. The bathymetry was derived from Admiralty Navigation Charts. A time step of 20 s was chosen. The model was run for 25 tidal cycles to achieve a stable time-periodic solution. After establishing the time-periodic regime, the model run was continued for a 29-day period; thereafter a harmonic analysis was performed on the tidal elevation and velocity so that the cotidal charts and the maps of tidal ellipse parameters and tidal energy budget characteristics for the M_2 and S_2 constituents could be constructed.

3. Modelling Results

The calculated cotidal charts for the M_2 and S_2 tidal waves are outlined in Figure 2. The M_2 chart shows a qualitative similarity with the empirical cotidal chart presented by *Candela et al.* [1990]; the S_2 chart displays the findings derived by the same authors from analysis of tide gauge and bottom pressure observations. In particular, these charts show a more than

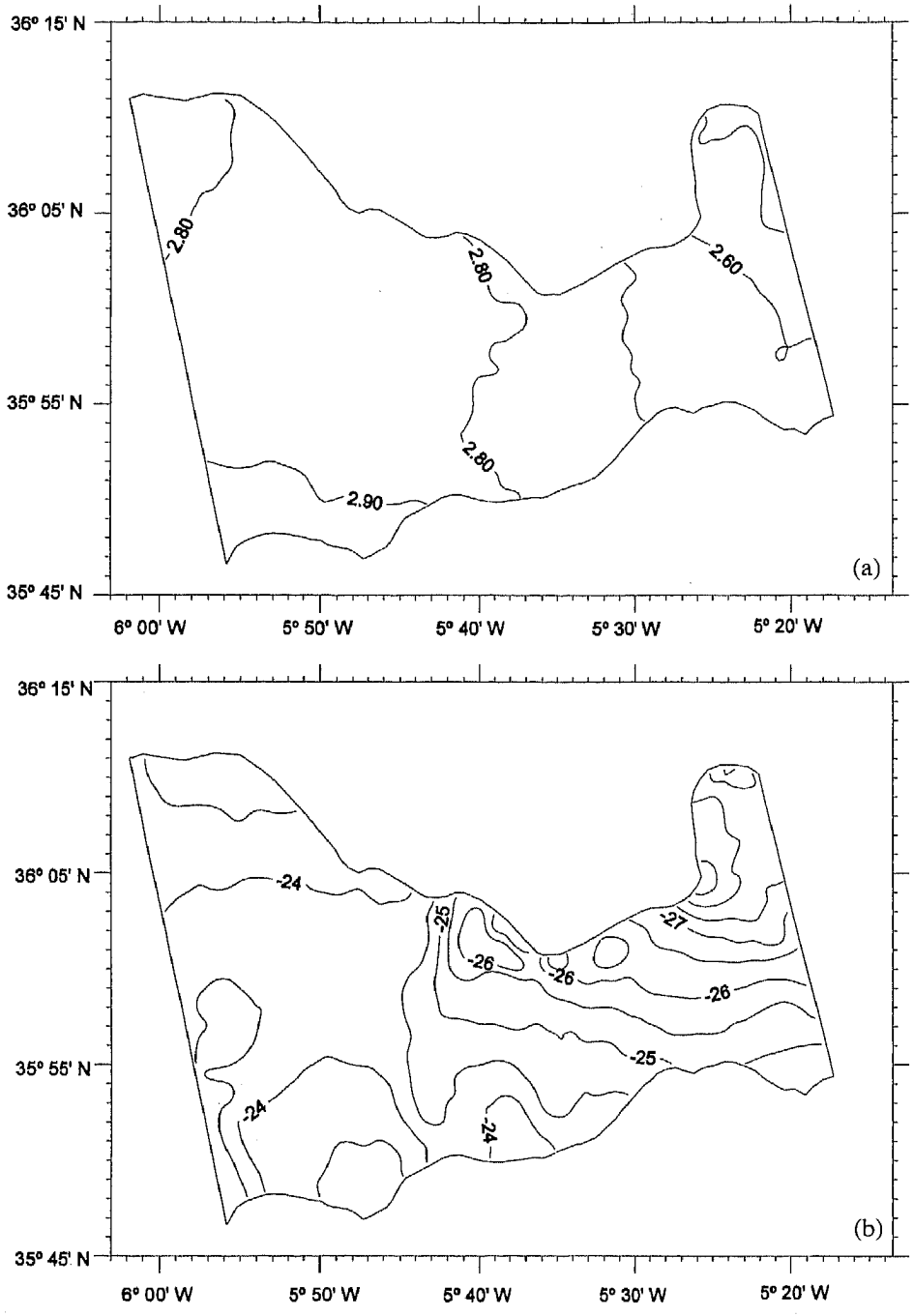

Figure 3. (a) Amplitude ratio and (b) phase difference, in degrees, between the M_2 and S_2 surface tides.

twofold reduction in the M_2 amplitudes between the western and eastern ends of the Strait of Gibraltar as well as their invariability in the across-strait direction, a small change in the M_2 phases along the strait with a clear propagation southwestward, and also fairly constant amplitude ratios and phase differences between the M_2 and S_2 constituents throughout the strait. As can be seen from Figure 3, the aforementioned amplitude ratios and phase differences vary within the strait in the range from 2.50 to 2.95 and from $-23.5°$ to $-28.0°$, respectively.

Good agreement between observed and predicted tidal constants is obtained (Table 1). The maximum differences between predicted and observed values do not exceed 7.0 cm (that is, ~10% in relative units) for amplitudes and 10° for phases. Making a quantitative comparison between the observed and predicted tidal ellipse parameters is difficult, since the former correspond to both barotropic tidal currents and internal tidal waves, while the latter correspond to barotropic tidal currents only. It is noteworthy to recall that separating barotropic and baroclinic tidal velocities either by a modal analysis (via solving the boundary value problem for the vertical structure of internal waves) or by a direct determination of the barotropic tidal velocities (via averaging observational data over depth) is prone to huge errors which makes their evaluation impossible. A more appropriate procedure is to extract that part of the tidal velocity which is coherent with the

Table 1. Comparison Between Observed and Predicted Amplitudes A and Phases g of Tidal Elevation

Site	Latitude North	Longitude West	M_2 Observed A, cm	M_2 Observed g, deg	M_2 Predicted A, cm	M_2 Predicted g, deg	S_2 Observed A, cm	S_2 Observed g, deg	S_2 Predicted A, cm	S_2 Predicted g, deg
Punta Gracia	36°05.4′	05°48.6′	64.9 ± 0.2	49 ± 0.5	70.4	55.0	22.3 ± 0.2	74.0 ± 1.0	24.7	78.8
DN	35°58′	05°46′	60.1	51.8	61.6	58.1	22.5	73.8	21.6	82.3
DS	35°54′	05°44′	54.0	61.8	57.4	61.2	21.1	83.3	20.2	85.8
SN	36°03′	05°43′	52.3	47.6	59.3	51.4	18.5	73.4	21.0	75.9
SS	35°50′	05°43′	57.1	66.8	58.9	67.3	20.6	92.3	20.4	91.4
DW	35°53′	05°58′	78.5	56.1	76.1	63.6	29.0	82.2	26.3	88.2
Kankoush	35°50.5′	05°41.0′	51.8 ± 0.4	69 ± 0.5	52.4	63.7	20.1 ± 0.4	90.0 ± 2.0	18.3	88.2
Tarifa	36°00.2′	05°36.4′	41.5 ± 0.2	57 ± 0.5	47.4	49.9	14.2 ± 0.2	85.0 ± 1.0	17.1	75.8
TA	36°01′	05°36′	41.2	41.2	45.8	49.8	14.7	67.9	16.6	75.8
Dp5	36°00′	05°34′	44.4	47.6	42.2	49.2	16.1	73.9	15.5	75.4
Punta Cires	35°54.7′	05°28.8′	36.4 ± 0.2	46.5 ± 0.5	36.7	56.8	14.1 ± 0.2	74.0 ± 1.0	13.7	81.6
AL	36°08′	05°26′	31.0	48.0	27.5	44.5	11.1	73.9	11.0	72.7
Punta Carnero	36°04.3′	05°25.7′	31.1 ± 0.2	47.5 ± 0.5	29.3	42.0	11.5 ± 0.2	71.0 ± 1.0	11.5	70.8
CE	35°53′	05°18′	29.7	50.3	29.3	48.2	11.4	75.6	11.1	73.1

Sources are *García Lafuente* [1986] and *Candela et al.* [1990]. Here ± indicates standard errors. Station locations are shown in Figure 1.

tidal elevation. This procedure was used by *Candela et al.* [1990] for separating the combined (M_2 and S_2) barotropic signal from current observations obtained during the Gibraltar Experiment. However, the individual M_2 and S_2 barotropic tidal velocities were not extracted. This step was made by *Mañanes et al.* [1998]. By applying a least squares harmonic analysis to the barotropic signal, they evaluated the amplitudes and the phases of both the M_2 and S_2 barotropic tidal velocities at 3 out of 11 current meter moorings available in the Gibraltar Experiment. Their estimates together with predicted values are presented in Table 2.

Table 2 shows that the agreement between observed and predicted values is rather good for phases and not good for amplitudes. This is due mainly to uncertainties in both the observed amplitudes and model deficiencies. In fact, the observed amplitude of the barotropic tidal velocity was defined by *Mañanes et al.* [1998] as the amplitude of the barotropic signal at a depth of 30 m at station M8 and as the average of the barotropic signal amplitudes at depths of 54 and 193 m at station M7 and of 110, 140 and 180 m at station M3. Because the amplitudes at these stations, especially at station M3, markedly vary with depth [*Candela et al.*, 1990; *Mañanes et al.*, 1998], in the case of a few measurement levels the average may provide only a crude estimate of the barotropic tidal velocity amplitude. Also, observations can show local features in the velocity field, whereas the model can resolve only the features with length scales being greater than the grid resolution.

Due to the lack of experimental information, there is no way to compare quantitatively the observed and predicted values of other barotropic tidal ellipse parameters. However, judging from Table 3, not only the semi-major axis M and the phase g, but also the orientation of the semi-major axis, Θ, the semi-minor axis m, and the sense of rotation which are produced by the model are in reasonable agreement with those obtained at all 11 current meter mooring locations in the strait.

The calculated fields of major and minor axes of the M_2 and S_2 barotropic tidal ellipses are shown together with the sense of rotation in Figure 4. The first point to note is the almost reversive character of the semidiurnal tidal currents in most parts of the Strait of Gibraltar; exceptions being the northwestern and eastern regions adjacent to the open boundaries. There, the ratio between major and minor semiaxes may be as much as 0.4. Extreme values of maximum current velocity (100–120 cm/s for M_2 and 30–40 cm/s for S_2) are predicted at the Camarinal Sill. To the west and east of the sill and in the Tarifa Narrows they do not exceed 80 cm/s for the M_2 tidal current and 25 cm/s for the S_2 tidal current. It is only in the Gibraltar Bay where maximum tidal velocities are weak (<10 cm/s for M_2 and <5 cm/s for S_2).

The most remarkable feature of the M_2 and S_2 tidal currents in the Strait of Gibraltar is the phase difference between maximum tidal velocity and elevation. As is apparent from Figure 5, it is ~90° throughout the central part of the strait. This feature is due to both end and topographic funnelling effects,

Table 2. Comparison Between Observed and Predicted Amplitudes of the M_2 and S_2 Barotropic Tidal Velocities at Selected Current Meter Mooring Locations

Station	M_2 Observed Amplitude	M_2 Observed Phase	M_2 Predicted Amplitude	M_2 Predicted Phase	S_2 Observed Amplitude	S_2 Observed Phase	S_2 Predicted Amplitude	S_2 Predicted Phase
M3	90.8	146.6	112	162	30.7	170.5	34	189
M7	24.8	159.5	40	155	12.4	177.9	12	181
M8	65.2	156.5	63	160	22.6	181.5	19	188

The source is *Mañanes et al.* [1998]; amplitudes are in centimeters per second, and phases are in degrees; the phase indicates the time of occurrence of maximum flood current (into the Mediterranean) with respect to universal time.

Table 3. Comparison Between Observed and Predicted Tidal Current Ellipse Parameters for the M_2 and S_2 Waves

	Depth, m	M_2				S_2			
		M, cm/s	m, cm/s	θ, deg	g, deg	M, cm/s	m, cm/s	θ, deg	g, deg
				Station M1					
Predicted	...	96	−7	351	158	29	−2	351	181
Measured	143	85	−5	353	133	31	−2	353	159
	156	81	−6	340	133	29	−2	340	159
	167	77	−6	351	132	28	−2	351	158
	215	44	−2	344	124	16	−1	344	150
				Station M2					
Predicted	...	108	−7	7	164	33	−4	7	189
Measured	90	115	2	3	141	41	11	3	168
	112	111	4	8	155	40	−1	8	181
	123	112	−3	11	154	40	−3	11	180
	135	118	−7	17	156	42	−2	17	182
	143	106	−6	14	154	38	−3	14	180
	153	113	−9	17	153	41	−5	17	179
	181	99	−14	20	132	36	0	20	158
	254	79	1	30	133	28	1	30	159
	306	58	3	43	133	21	−1	43	159
				Station M3					
Predicted	...	112	−6	9	162	34	−3	9	189
Measured	110	115	−3	9	146	41	−2	9	172
	127	101	−6	12	144	36	−2	12	170
	140	104	−5	12	148	37	−1	12	174
	172	49	−2	18	146	18	−1	18	172
	180	66	−3	12	145	24	0	12	171
				Station M7					
Predicted	...	40	−13	25	155	12	−3	20	181
Measured	54	21	−6	20	208	8	1	20	234
	193	37	2	26	139	13	1	26	165
				Station M8					
Predicted	...	63	−0.7	15	160	19	0.8	13	188
Measured	30	67	3	15	156	24	1	15	182
				Station M9					
Predicted	...	71	3	26	169	21	−0.1	24	191
Measured	58	49	2	13	189	18	1	13	215
	159	61	1	17	124	22	1	17	150
				Station F3					
Predicted	...	107	−8	6	164	33	−4	7	189
Measured	63	111	3	12	143	40	1	12	169
	126	115	−5	16	145	41	−2	16	171
	165	77	−6	29	125	28	−2	29	151
	225	81	0	40	130	29	0	40	157
				Station F4					
Predicted	...	45	−4	16	161	14	−0.7	16	184
Measured	60	49	−2	24	182	18	−1	24	208
	120	37	−1	19	135	13	0	19	161
				Station TN					
Predicted	...	68	7	25	157	20	0.8	22	182
Measured	16	25	2	22	154	7	2	17	146
	24	26	1	20	153	8	1	17	147
	32	36	2	17	152	12	1	17	153
	40	41	1	16	152	15	0.4	15	153
	48	40	0	15	152	15	0	14	149
	56	39	−1	13	151	16	−0.2	13	144
	64	38	−1	11	149	15	−0.2	12	140
	72	37	−2	10	145	15	−0.3	11	137
	80	37	−2	10	140	14	−0.2	10	135
	88	38	−2	9	135	14	−0.3	9	133
	96	39	−2	8	131	13	−0.1	8	131
	104	40	−2	7	128	13	0	7	130
	112	41	−2	6	125	13	0.1	7	128
	120	42	−2	5	122	13	0.4	7	126

Table 3. (continued)

	Depth, m	M_2				S_2			
		M, cm/s	m, cm/s	θ, deg	g, deg	M, cm/s	m, cm/s	θ, deg	g, deg
				Station F4					
Predicted	...	64	9	16	154	20	0.4	16	182
Measured	170	58	−5	356	139	29	−1.8	358	170
	180	59	−5	355	136	29	−1.9	358	167
	190	59	−5	355	133	28	−1.8	358	165
	200	60	−5	355	131	28	−1.6	358	163
	210	60	−5	355	129	27	−1.5	358	161
	220	60	−5	355	128	27	−1.5	357	159
	230	60	−5	355	126	27	−1.4	357	157
	240	60	−5	355	125	27	−1.4	357	156

Sources are *Candela et al.* [1990] and *Ruíz Cañavante* [1994]. The sign of the semiminor axis indicates the sense of rotation of the tidal current and is positive counterclockwise; orientation corresponds to maximum flood current (into the Mediterranean) and is measured counterclockwise from the east. For definition of phase, see Table 2.

the latter of which for supercritical convergence and weak friction (the case typical of the Strait of Gibraltar) causes a progressive wave to be transformed into a standing wave with a phase difference of ~90° between tidal velocity and elevation. One additional comment should be made about the terms "progressive waves" and "standing waves." These conventional terms are appropriate only to inviscid waves in channels of uniform width and depth. For convergent channels with friction, they may be referred to the progressive and standing components of mixed, progressive-standing waves.

The fact that topographic funnelling may account for a nearly 90° phase difference between tidal velocity and elevation is illustrated in Appendix B via the example of a simple model problem on tidal propagation in a weakly dissipative, narrow channel with small variations in geometry and the topographic length scale being much smaller than a characteristic tidal wavelength. The sensitivity results to changing geometry, which are presented in section 4, also support this view. These results show that topographic funnelling does make a contribution to the formation of the semidiurnal surface tides in the strait. However, in short and narrow enough straits, like the Strait of Gibraltar, it is difficult, whenever possible, to distinguish between the topographic funnelling and end effects. The reason is that the small (relative to tidal wavelength) along-strait dimensions predetermine the overlapping of the signals induced by the two factors at open boundaries. This, in turn, makes such a distinction difficult in the interiors of the straits. Therefore all that can be said in a given case is that both the end and topographic funnelling effects are responsible for the gross features in the fields of tidal characteristics in the strait and, in particular, for the occurrence of a vast area with a phase difference of about 90°. The same is also true for mesoscale features, although intuitively, the major role in their formation is to belong to topographic funnelling.

The mere fact that the phase difference is nearly 90° implies vanishing of the mean (over a tidal cycle) energy flux. The model results displayed in Figure 6 indicate that in most parts of the Strait of Gibraltar the mean tidal energy flux per unit length is indeed small. Its maximum value is -3.4×10^5 W/m for the M_2 tidal wave and -0.42×10^5 W/m for the S_2 tidal wave (hereinafter, we shall use the minus sign to mean a westward direction of the flux). These values occur only in the vicinity of the eastern boundary. At the Camarinal Sill and in the central region of the Tarifa Narrows in particular, they vary from -0.2×10^5 to -2.8×10^5 W/m for M_2 and from -0.02×10^5 to -0.28×10^5 W/m^2 for S_2.

Another interesting feature of the considered fields is that the directions for the M_2 and S_2 mean tidal energy fluxes in the vicinities of the eastern and western boundaries of the strait exhibit clearly defined changes. These changes are associated with a peculiar kind of dipole structure (i.e., two neighboring zones with opposing tendencies for the phase difference to vary; see Figure 5) suggesting the existence of eddies that are located in the adjacent regions of the Mediterranean Sea and the North Atlantic and enclose in part the Strait of Gibraltar.

We would like to call attention to the following fact: As can be seen from Figure 6, the mean tidal energy flux is structured in the cross-strait direction such that it decreases by one order of magnitude when approaching the coast. Accordingly, the value of $(8 \pm 10) \times 10^8$ W for the M_2 net tidal energy flux obtained by *Candela et al.* [1990] at the Camarinal Sill and applied to the entire sill cross section, leads to an overestimate. However, a not too great significance should be attached to this fact because, as has been pointed out by *Candela et al.* [1990], the above estimate cannot be regarded as being statistically reliable since the mean and standard deviation are comparable. Moreover, it should be emphasized that this estimate was obtained directly from current velocity and bottom pressure data, without first separating barotropic and baroclinic velocity components. Therefore the above estimate for the M_2 net tidal energy flux is more likely to correspond to the combined (surface plus internal) M_2 tide rather than the surface M_2 tide only. In this context, it would be of interest to clear up, first, what the net tidal energy fluxes for the M_2 and S_2 surface tides are and, second, how these fluxes are modified by means of interactions with the M_2 and S_2 internal tides. We shall provide an answer to the first issue. The second one cannot be clarified by the model considered here, because it does not include baroclinic effects. Studies to provide estimates for the energy exchange between surface and internal tides using a 2-D, high-resolution, nonlinear, two-layer, boundary-fitted coordinate model are in progress and will be reported in the future.

There are two more model estimates (16×10^8 W and 6.5×10^8 W) for the M_2 net tidal energy flux through the Strait of Gibraltar, obtained by *Tsimplis et al.* [1995] and *Lozano and Candela* [1995]. The first estimate was found from a tidal model for the Mediterranean Sea by fitting the harmonic con-

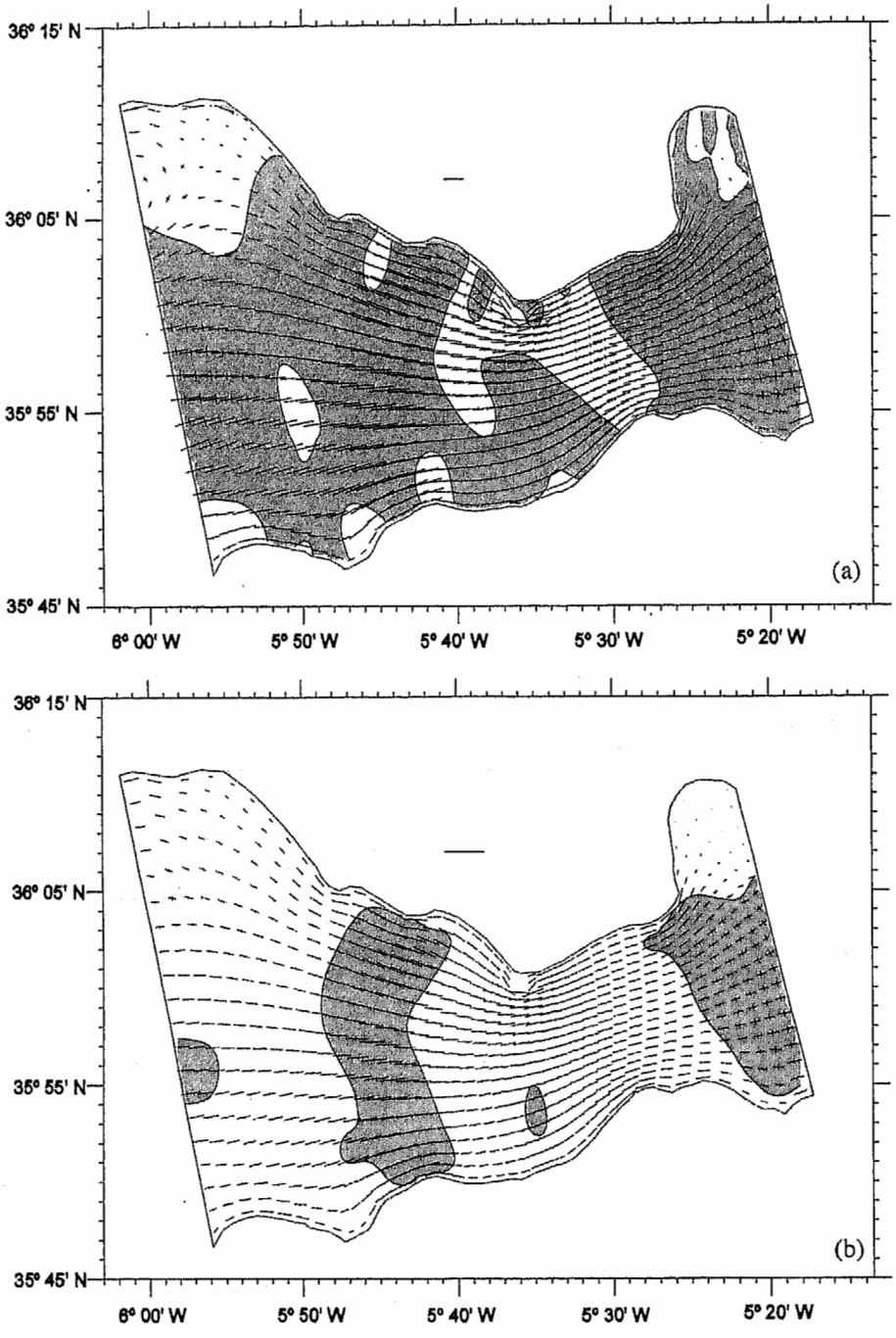

Figure 4. Major and minor axes of tidal ellipses and sense of rotation of tidal velocities for (a) M_2 and (b) S_2. Velocity scales (1 m/s) are indicated at the top of the figures; shaded and unshaded regions correspond to clockwise and anticlockwise rotation, respectively.

stants of tidal elevation and velocity in the strait so as to achieve the best agreement between predicted and observed tidal amplitudes and phases at the Mediterranean tide gauge stations. As a result, the harmonic constants turn out to be different from those observed in the strait. A certain tuning was also used in the tidal model of *Lozano and Candela* [1995], taking into account a change in the observed tidal amplitudes and phases in the Gulf of Cádiz. In addition, the Strait of Gibraltar was represented in their model as a narrow, rectangular channel, and thus the effect of topographic funnelling was neglected. Hence the estimates for the net tidal energy flux can be considered only as approximate which is, however, not essential.

The main point to make here is that the model estimates above suggest a mean transport of tidal energy from the Strait of Gibraltar into the Mediterranean Sea. However, this direction of the net tidal energy flux is inconsistent with the existing cotidal charts of the Strait of Gibraltar in the sense that this flux is in the opposite direction to the tidal phase propagation. The model results presented in Figure 6 show that the general direction for the M_2 and S_2 mean tidal energy fluxes is to the west throughout much of the strait, with visible deviations from

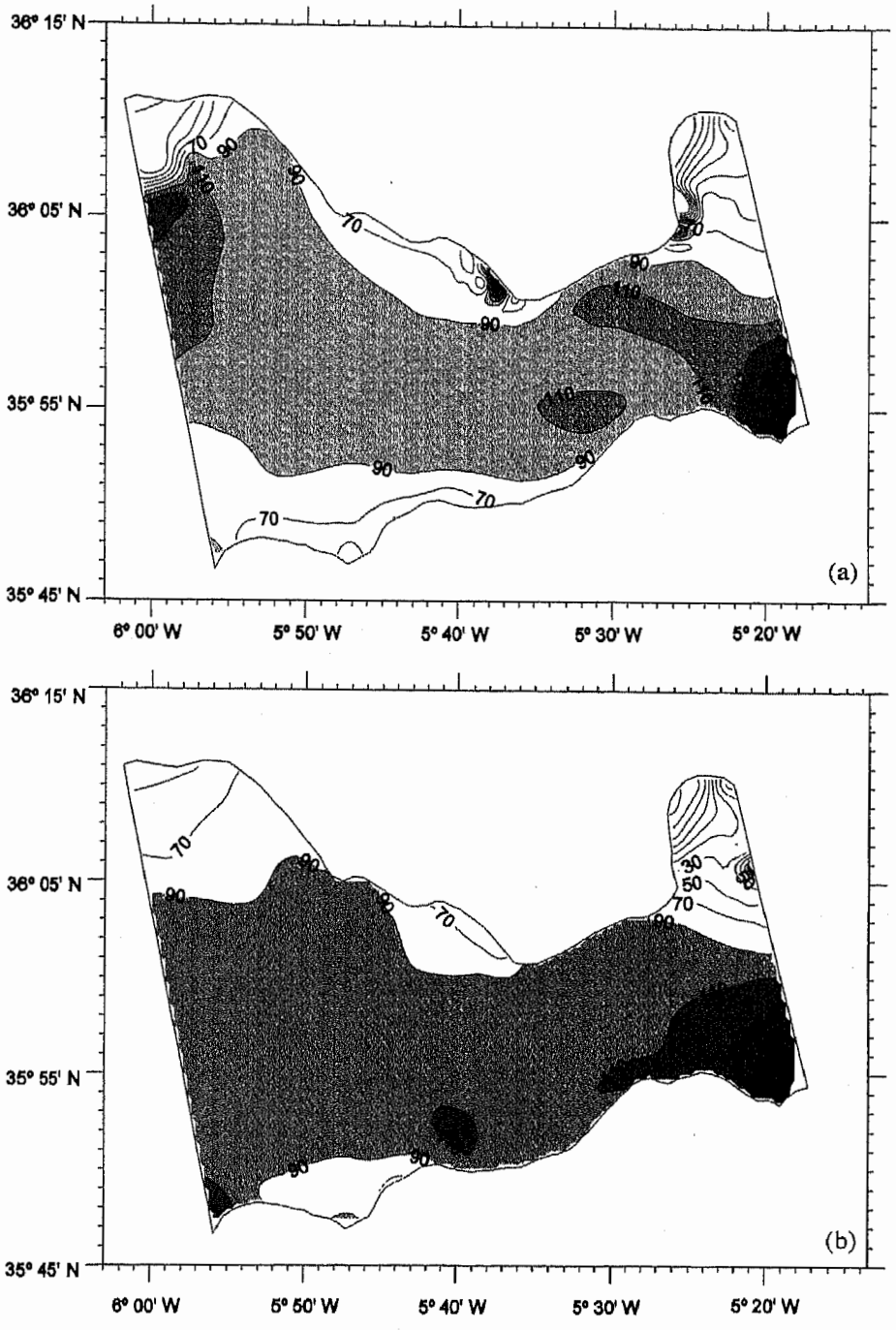

Figure 5. Phase difference (degrees) between maximum tidal velocity and tidal elevation for (a) M_2 and (b) S_2. The regions where the phase difference exceeds 90° are shaded.

this direction at the Camarinal Sill and in the Tarifa Narrows. There exists some evidence in support of the conclusion on the general direction for the M_2 and S_2 net tidal energy fluxes to the west. According to *Candela et al.* [1990], ebb currents (toward the Atlantic) precede high waters in the strait. It follows that the phase difference between tidal velocity and elevation is greater than 90° everywhere, suggesting a general westward direction for the net tidal energy flux. This fact may be regarded as the indication of an elevation node for each of the semidiurnal surface tides in the western part of the Mediterranean. The possibility of the existence of this node has been speculated by *Candela et al.* [1990]; see also *Defant* [1961].

We recall that not only the direction but also the magnitude of the mean tidal energy flux varies along the Strait of Gibraltar. From Figure 7 the general tendency is evident for a decrease in the net tidal energy flux from the eastern to the western end of the strait. It is also apparent that the divergence of the net tidal energy flux in the region of the Camarinal Sill takes maximum values, suggesting a strong local sink of tidal energy.

As can be seen from Figure 8, the tidal energy dissipation at

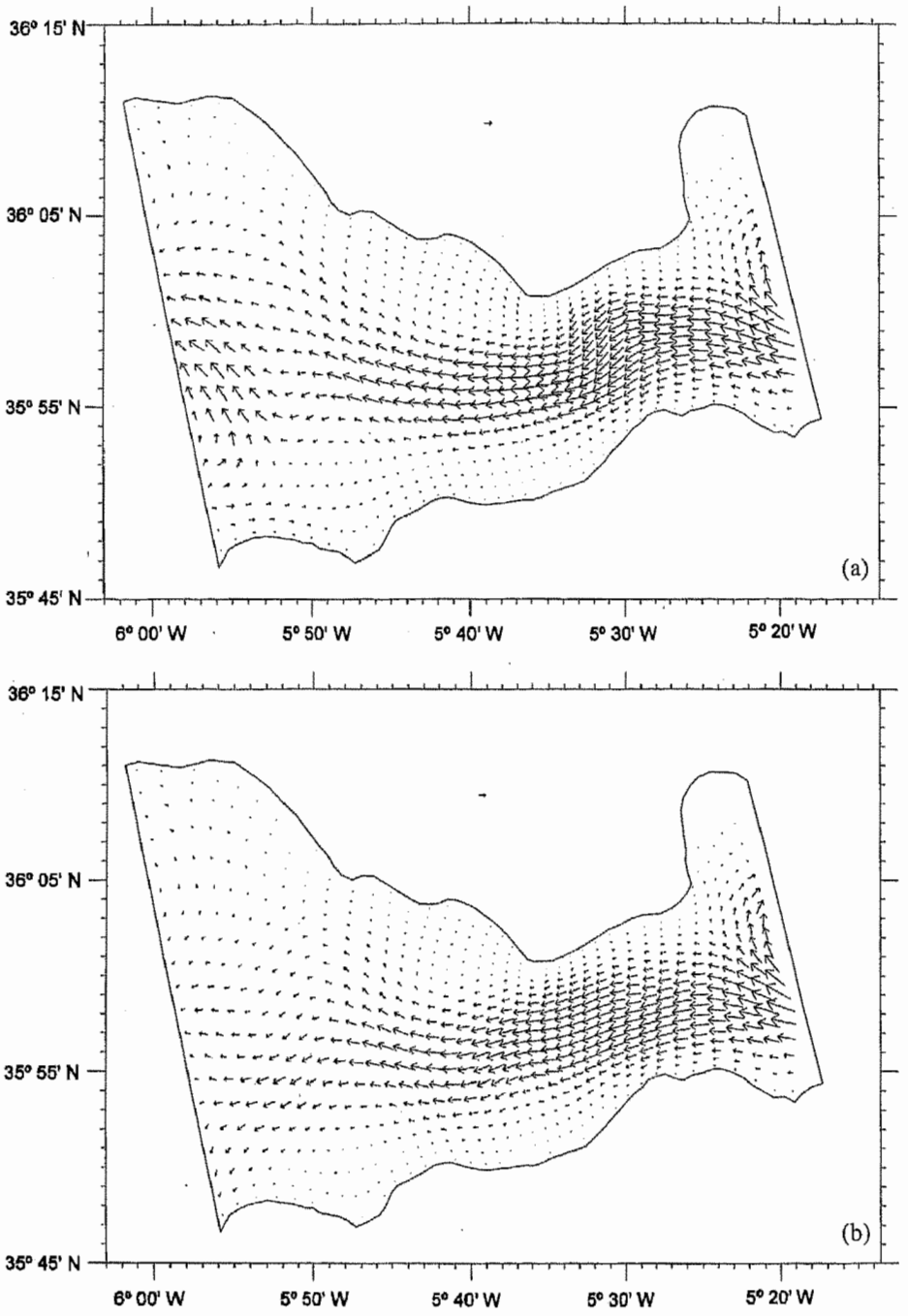

Figure 6. Mean tidal energy flux per unit length for (a) M_2 and (b) S_2. Flux scales (10^5 W/m for M_2 and 10^4 W/m for S_2) are indicated at the top of the figures.

the Camarinal Sill greatly exceeds the predicted values in the remaining parts of the Strait of Gibraltar and has a maximum in the coastal regions due to increasing tidal current velocities there. Considering the fact that this local sink occupies a sizeable area of the strait, it is not surprising that this sink controls the total tidal energy dissipation, which is estimated to be 5.5×10^8 W for the M_2 tidal wave and 0.2×10^8 W for the S_2 tidal wave. Note that the model does not include any other dissipative mechanisms except for bottom friction. Therefore the derived estimates for tidal energy dissipation should be recognized as tentative and intended to provide an approximate magnitude of tidal energy losses in the strait. On the basis of these estimates we conclude that the M_2 total tidal energy dissipation in the Strait of Gibraltar is nearly equal to, or several times greater than, its estimate for the Mediterranean Sea, depending which of the two existing model estimates ($\sim 8 \times 10^8$ W after *Tsimplis et al.* [1995], or 0.94×10^8 W after *Lozano and Candela* [1995]) is chosen for comparison.

4. Numerical Experiments

It is known that the only factor controlling the direction of mean tidal energy flux is the phase difference between tidal velocity and elevation. Because the phase difference in most of

the Strait of Gibraltar is slightly greater than 90°, thereby predetermining the general direction for the mean tidal energy flux westward, the question arises of how robust this result is. That is, can inaccuracies in the prescribed boundary forcing or ignoring the appropriate astronomical forcing give rise to the eastward directed M_2 and S_2 mean tidal energy fluxes? In addition, it would be also desirable to clarify the role of the end and topographic funnelling effects in the formation of the semidiurnal surface tides in the Strait of Gibraltar. All this, plus strong recommendations of the reviewers, impelled us to carry out a set of numerical experiments on the sensitivity of the solution to variations in boundary and astronomical forcings and changing geometry.

4.1. Sensitivity to Boundary Forcing

Recall that the tidal constants at the open boundary grid nodes were derived by interpolation of observed values at two points of each boundary. One way of examining how sensitive the model results are to boundary forcing is to give up setting the tidal elevations at the open boundaries and to move these boundaries beyond the limits of the domain of influence of the strait. In doing so, we cannot avoid the problems of defining the influence domain and setting boundary conditions at its open boundaries. A solution to the first of the problems may be found, at least as a rough approximation, from the analytical model of *Rocha and Clarke* [1987]. Concerning the problem of specifying the open boundary conditions, this requires some comments. If an insufficient number of bottom pressure observations is available at the open boundaries, the tidal elevations at these boundaries can be derived, in principle, from observations in the interior of the region of interest by applying inverse techniques. This approach, however, is not without disadvantages. As was shown, for example, by *Foreman et al.* [1980], the problem of deriving boundary conditions from observations within the region of interest is ill posed. This results in unrealistically great tidal elevations at the open boundaries when using direct substitution algorithms [*McIntosh and Bennett*, 1984]. Moreover, the boundary values of tidal elevation are very sensitive to small errors in observational data. This defect can be eliminated by adding a penalty function to be minimized with a term proportional to the variance of the difference between predicted tidal elevation at the open boundary and a certain first guess. However, the quality of the solution thus obtained depends critically on the coefficient of proportionality (weight) in the added term. In the absence of a priori information on the accuracy of the first guess, an adequate choice of the coefficient of proportionality is a rather delicate problem. There are several algorithms for solving this problem, one of them being Wahba's cross validation. However in our case, where the number of available observations is much less than the number of open boundary grid nodes at which tidal elevations have to be provided, it is unlikely that these algorithms can be applied successfully.

For the reasons given above, we prefer to resort to the simplest way. Namely, the tidal constants at the western boundary grid nodes are obtained interpolating the observed values at three measurement points (tide gauge stations Trafalgar and Espartel and bottom pressure station DW), rather than using the first two of them only as is done in the control solution described in section 3. All the other conditions of the experiment, referred to as experiment 2, are retained with no modifications.

The resulting solution for the M_2 and S_2 surface tides is identical in a qualitative sense to the control solution. As expected, some quantitative differences between the two solutions are mainly concentrated in the western part of the strait, but even there the differences are modest. This can be seen when comparing the predicted elevation amplitudes and phases at tide gauge and pressure observation locations with those corresponding to the control solution (Table 4). From this table we notice that the maximum differences do not exceed 3.0 cm for amplitudes and 5.0° for phases. Because of changes in the phase difference between tidal velocity and elevation the tidal energy budget characteristics vary as well. In particular, if in the control solution the net tidal energy fluxes at the eastern and western boundaries of the strait are -20.2×10^8 W and -14.7×10^8 W for M_2 and -2.3×10^8 W and -2.1×10^8 W for S_2, then in experiment 2 they are -13.2×10^8 W and -5.0×10^8 W for M_2 and -1.6×10^8 W and -1.3×10^8 W for S_2, respectively. More importantly, in experiment 2 the M_2 and S_2 mean tidal energy fluxes (Figure 9) and the M_2 and S_2 net tidal energy fluxes (Figure 7) are directed westward as in the control solution.

Incidentally, in the control solution the root-mean-square differences between the predicted and observed tidal elevation amplitudes and phases are 2.9 cm and 4.7° for M_2 and 1.2 cm and 3.9° for S_2, whereas in experiment 2 they are 3.9 cm and 4.7° for M_2 and 1.4 cm and 3.6° for S_2. That is, the two-point interpolation of tidal constants at the western boundary of the strait provides a better agreement than the three-point interpolation. This is the reason why the former was employed for setting the boundary forcing in the control solution.

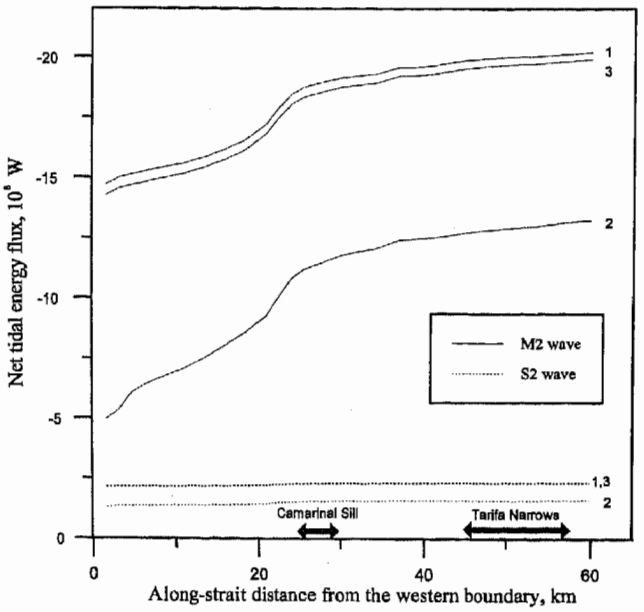

Figure 7. Variations in the net tidal energy flux along the Strait of Gibraltar. The values shown in the figure correspond to the integral (over a cross-sectional curvilinear grid line) transport of tidal energy; the minus sign corresponds to westward flux; and lines 1, 2, and 3 apply to the control solution and experiments 2 and 3, respectively.

4.2. Sensitivity to Astronomical Forcing

The purpose of this experiment is to check the possibility for the mean tidal energy flux to be reorganised under astronomical forcing. Since the linear sizes of the Strait of Gibraltar are

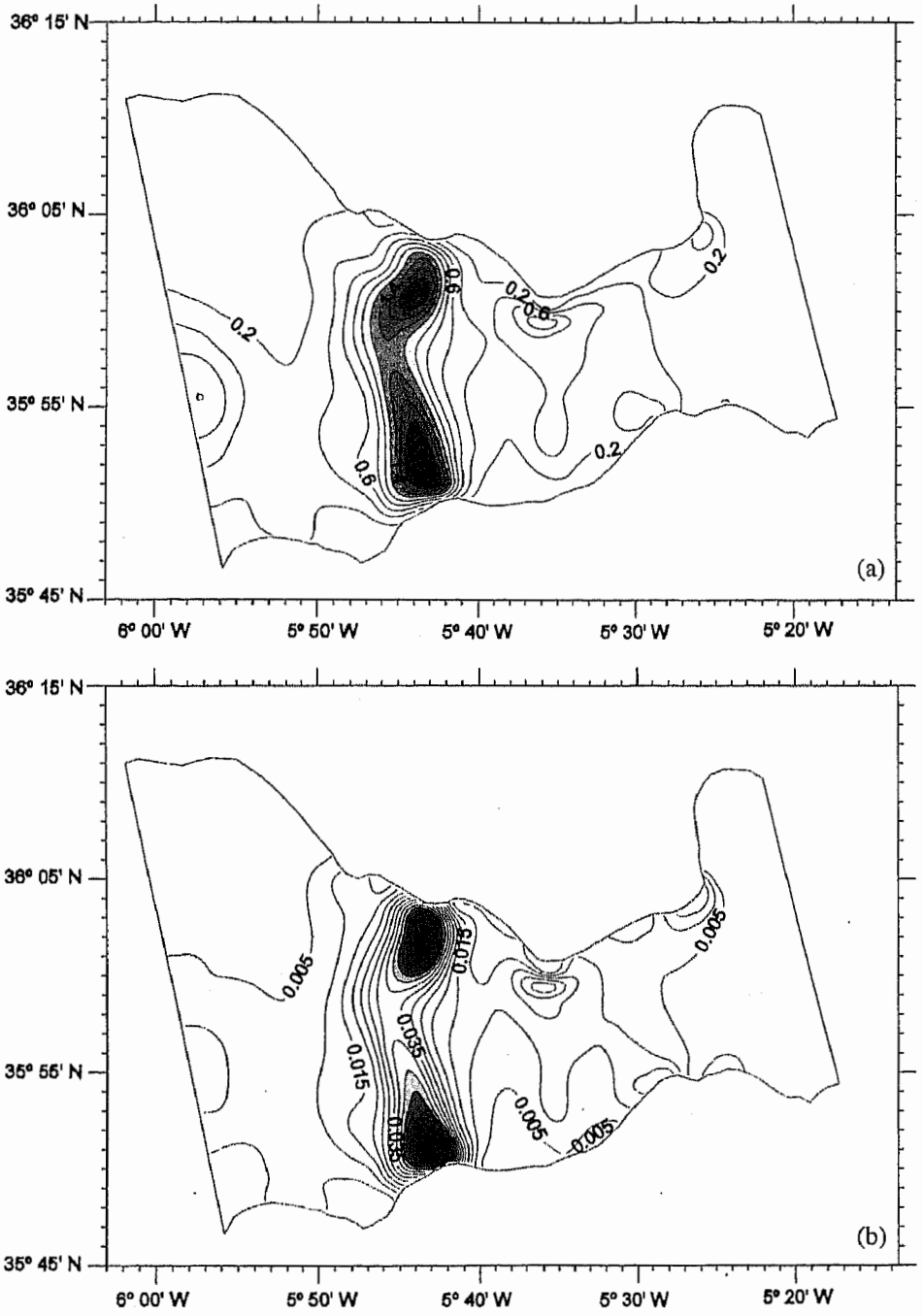

Figure 8. Tidal energy dissipation (W/m^2) for (a) M_2 and (b) S_2. Regions of enhanced dissipation are shaded.

much smaller than the length scale of the tide-generating force, it may be suggested that astronomical forcing does not significantly affect the tidal dynamics in the strait. This is confirmed by the results of experiment 3. In this experiment, taking into account the effect of astronomical forcing, a proper term arising from the equilibrium tide was added to the momentum equations, other conditions being unchanged.

As can be seen from Table 4, the tidal elevation amplitudes and phases at tide gauge and bottom pressure observation sites show maximum differences of 0.6 cm and 0.9°, respectively. Again, only quantitative changes of the tidal energy budget characteristics are detected with respect to the control solution. These changes are small, smaller even than those found in experiment 2. The net tidal energy fluxes at the eastern and western boundaries of the strait and the total mean tidal energy dissipation are estimated to be -19.9×10^8 W, -14.2×10^8 W, and 5.7×10^8 W for M_2 and -2.3×10^8 W, -2.1×10^8 W, and 0.2×10^8 W for S_2, respectively. Clearly, they differ only slightly from the values in the control solution.

4.3. Sensitivity to Changing Geometry

In order to clarify the relative significance of the end and topographic funnelling effects, two numerical experiments were carried out. In contrast to the control solution, the fol-

Table 4. Model Amplitudes and Phases of Tidal Elevation at Tide Gauge and Bottom Pressure Observation Sites for the Control Solution (Experiment 1) and Experiments 2 and 3

	M_2 Amplitude, cm			M_2 Phase, deg			S_2 Amplitude, cm			S_2 Phase, deg		
Site	1	2	3	1	2	3	1	2	3	1	2	3
Punta Gracia	70.4	73.1	70.1	55.0	51.3	55.0	24.7	26.5	24.6	78.8	75.8	78.9
DN	61.6	63.1	61.4	58.1	54.0	58.0	21.6	23.1	21.6	82.3	78.5	82.3
DS	57.4	59.2	57.3	61.2	56.4	61.1	20.2	21.6	20.2	85.8	82.1	85.8
SN	59.3	60.4	58.9	51.4	47.7	51.5	21.0	22.4	21.0	75.9	72.4	76.2
SS	58.9	60.3	58.7	67.3	62.3	67.2	20.4	22.0	20.3	91.4	87.4	91.4
DW	76.1	...	76.2	63.6	...	63.6	26.3	...	26.3	88.2	...	88.3
Kankoush	52.4	54.1	52.2	63.7	59.9	63.6	18.3	19.7	18.3	88.2	85.2	88.1
Tarifa	47.4	48.0	47.2	49.9	47.0	50.3	17.1	17.9	17.1	75.8	72.9	75.9
TA	45.8	46.5	45.8	49.8	46.8	49.9	16.6	17.3	16.6	75.8	73.1	75.9
Dp5	42.2	42.7	42.2	49.2	46.5	49.3	15.5	16.1	15.5	75.4	72.9	75.5
Punta Cires	36.7	37.6	36.6	56.8	54.9	56.6	13.7	14.3	13.7	81.6	80.2	81.6
AL	27.5	27.6	27.6	44.5	44.6	44.8	11.0	11.0	11.0	72.7	72.4	72.6
Punta Carnero	29.3	29.1	29.3	42.0	41.5	41.9	11.4	11.4	11.5	70.8	70.2	70.6
CE	29.3	29.5	29.3	48.2	48.0	48.1	11.1	11.1	11.1	73.1	73.4	73.1

lowing conditions were employed: in the first experiment, the depth was taken to be 240 m, whereas in the second experiment the strait was approximated by a rectangular channel with a depth of 240 m and a width of 26 km. As before, all other conditions, including boundary forcing, were prescribed identical to those employed in the control solution.

Notice that the assumption of identical boundary forcing implies implicitly that the tidal elevations at the open boundaries are governed only by the tides in the adjacent basins and are not affected by the strait's geometry effects. Strictly speaking, this is not the case. However, on extending the model domain, we are again facing the problem of how to specify the tidal elevations at the open boundaries of the extended domain. Attempts to solve this problem by inverse techniques based on observations within the strait will not furnish the desired results because these observations are also disturbed by the strait's geometry effects. Therefore, recognizing all the limitations of our approach, we took the tidal elevations at the open boundaries to be identical to those specified in the control solution. Regardless of those limitations, it can nevertheless provide qualitative insight into the problem we are interested in.

In both experiments, mesoscale features in the spatial distribution of the tidal characteristics are now extinct, while the gross features such as the southwestern tidal phase propagation and the westward direction of the mean tidal energy fluxes remain similar to those that are detectable in the control solution. The net tidal energy fluxes through the eastern and western boundaries are, respectively, -14.4×10^8 W and -6.7×10^8 W for M_2 and -1.6×10^8 W and -1.2×10^8 W for S_2 in the first experiment, and -20.5×10^8 W and -14.1×10^8 W for M_2 and -1.9×10^8 W and -1.6×10^8 W for S_2 in the second one. Accordingly, in the case of constant depth the total mean tidal energy dissipation is 7.7×10^8 W for M_2 and 0.4×10^8 W for S_2, whereas in the case of constant depth and width it equals 6.4×10^8 W for M_2 and 0.3×10^8 W for S_2.

It should be noted that deviations from the phase difference of 90° in the central part of the model strait become greater than those obtained in the control solution. In other words, in the cases considered, the semidiurnal surface tides more closely resemble progressive waves than standing waves, thereby implying a suppression of the topographic funnelling effect.

Thus the numerical experiments discussed provide support for the M_2 and S_2 mean tidal energy fluxes to be directed westward regardless of variations in tidal elevations at the western boundary of the Strait of Gibraltar, the inclusion of astronomical forcing, and changes in the Strait's geometry. In this sense, the above result may be recognized as robust. As is evident from the foregoing discussion, both the end and topographic funnelling effects are responsible for a general westward direction for the M_2 and S_2 mean tidal energy fluxes. Which of these effects is prevailing is not evident. However, even if topographic funnelling cannot lead to a radical reorganisation of the tidal dynamics in the strait, it can give rise to mesoscale features in the fields of tidal characteristics and especially tidal energy budget characteristics, the features like those depicted in Figures 6–8.

5. Conclusions

A 2-D, nonlinear, boundary-fitted coordinate model is applied for simulating the M_2 and S_2 semidiurnal surface tides in the Strait of Gibraltar. The tidal simulation is carried out on a grid with a nominal spatial resolution of 0.5 km. The model shows good agreement with the tidal amplitudes and phases derived from tide gauge and bottom pressure measurements. The predicted tidal ellipse parameters are in qualitative agreement with those obtained during the Gibraltar Experiment.

The model reproduces all of the known features of the spatial structure of the M_2 and S_2 tidal waves. Namely, a more than twofold decrease in amplitudes and slight variations in phases along the strait, a prevailing propagation of phases southwestward, and a phase difference of nearly 90° between tidal velocity and elevation at the Camarinal Sill, as well as nearly constant amplitude ratios and phase differences between the M_2 and S_2 tidal elevations throughout the strait, are obtained.

At the same time the model has revealed some new features in the tidal dynamics of the Strait of Gibraltar. These features not only eliminate the contradiction between the observed southwestern tidal phase propagation and a commonly used tidal energy transport eastward, but can also change the traditional view of the role of the Strait of Gibraltar in the formation of the semidiurnal surface tides in the Mediterranean Sea. In particular, it has been found that the general direction for the mean tidal energy flux is to the west, with a clear increase

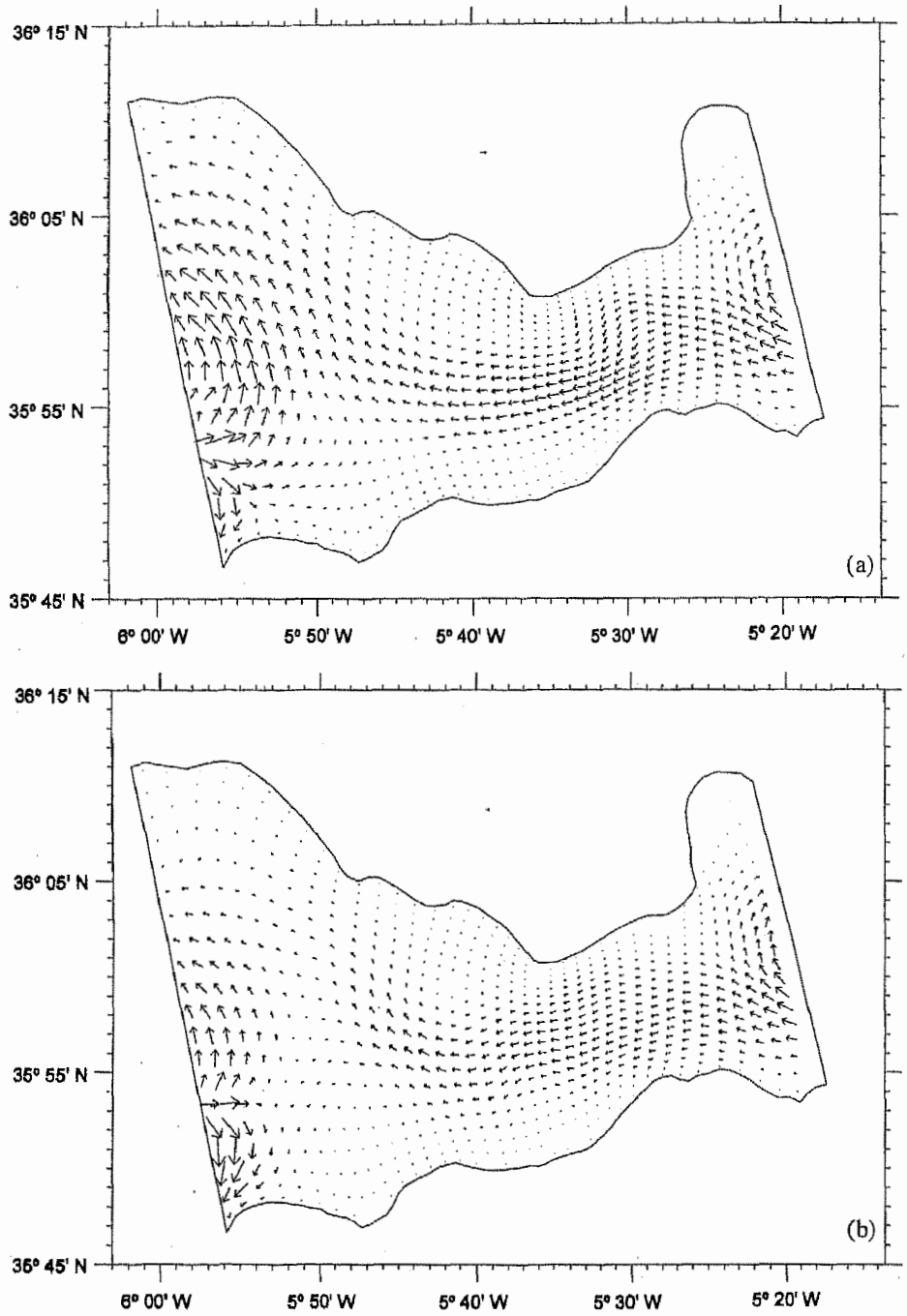

Figure 9. Mean tidal energy flux per unit length for (a) M_2 and (b) S_2 for experiment 2. Flux scales are identical to those indicated in Figure 6.

in the divergence of the net tidal energy flux in the vicinity of the Camarinal Sill. This increase leads to the appearance of a strong local sink of tidal energy due to bottom friction. The tidal energy dissipation is markedly greater at the Camarinal Sill than anywhere else, thereby determining the total tidal energy dissipation in the Strait of Gibraltar as a whole. The total tidal energy dissipation in the strait is estimated to be 5.5×10^8 W for the M_2 tidal wave and 0.2×10^8 W for the S_2 tidal wave. These estimates are of the same magnitude as, if not greater than, those in the Mediterranean Sea.

Another interesting feature in the spatial structure of the M_2 and S_2 tidal waves is the existence of a vast area with a ~90° phase difference between tidal velocity and elevation. This feature may be attributed to both the end and topographic funnelling effects. The latter in the case of supercritical convergence and weak friction, which are typical of the Strait of Gibraltar, causes a progressive wave to be transformed into a standing wave with a phase difference of ~90° between tidal velocity and elevation. That this is so is suggested by the solution of a simple model problem describing tidal propagation in a weakly dissipative, narrow channel with small variations in geometry and with topographic length scale much smaller than a characteristic tidal wavelength.

The sensitivity results to changing geometry reinforce the

statement that topographic funnelling does make a contribution to the formation of the semidiurnal tides in the Strait of Gibraltar but do not tell anything about the relative significance of the end and topographic funnelling effects taken separately. The reason is that the small (relative to the tidal wavelength) along-strait dimension predetermines the overlapping of the signals induced by the two factors at the open boundaries of the strait. This, in turn, means that it is difficult, whenever possible, with the model in use to draw a definite conclusion regarding the relative significance of the end and topographic funnelling effects in the interior of the strait. Such is an obvious shortcoming of the given model and, generally, any other models based on the use of empirical information for specifying boundary conditions. However, the purpose of the model is to produce the detailed cotidal charts and the detailed maps of tidal ellipse parameters and tidal energy budget characteristics for the semidiurnal surface tides in the region of interest. In this respect, the model may serve as a proper hydrodynamical interpolator of tidal data at the open boundaries of the strait. The results presented here show that it lives up to expectations.

Appendix A: Model Equations, Boundary Conditions, and the Method of Solution

The model equations are the depth-averaged tidal dynamics equations. In a boundary-fitted coordinate system these equations are

$$\zeta_t + J^{-1}[(JUH)_\xi + (JVH)_\eta] = 0 \tag{A1}$$

$$U_t + U(U_\xi + U\Gamma^1_{11} + V\Gamma^1_{12}) + V(U_\eta + U\Gamma^1_{12} + V\Gamma^1_{22}) = -gJ^{-2}(g_{22}\zeta_\xi - g_{12}\zeta_\eta) + J^{-1}f(g_{12}U + g_{22}V) - \tau_U/\rho H \tag{A2}$$

$$V_t + U(V_\xi + U\Gamma^2_{11} + V\Gamma^2_{12}) + V(V_\eta + U\Gamma^2_{12} + V\Gamma^2_{22}) = -gJ^{-2}(g_{11}\zeta_\eta - g_{12}\zeta_\xi) - J^{-1}f(g_{11}U + g_{22}V) - \tau_V/\rho H \tag{A3}$$

where ζ is the tidal elevation; U and V are the contravariant components of the depth-averaged velocity vector in the curvilinear coordinate system (ξ, η) which are related to the u and v components of the depth-averaged velocity vector in the Cartesian coordinate system (x, y) via the relationships $u = (Ux_\xi + Vx_\eta)$ and $v = (Uy_\xi + Vy_\eta)$; $\tau_U = \rho c_D G U$ and $\tau_V = \rho c_D G V$ are terms arising from the bottom stress parameterized by the quadratic resistance law, with the bottom friction coefficient $c_D = 2.5 \times 10^{-3}$; $G = (g_{11}U^2 + 2g_{12}UV + g_{22}V^2)^{1/2}$; H is the depth; ρ is the density of seawater; g is the acceleration due to gravity; $J = (x_\xi y_\eta - x_\eta y_\xi)$, $0 \neq J < \infty$, is the Jacobian; $g_{11} = (x_\xi^2 + y_\xi^2)$, $g_{22} = (x_\eta^2 + y_\eta^2)$, and $g_{12} = (x_\xi x_\eta + y_\eta y_\xi)$ are the covariant components of the metric tensor; $\Gamma^l_{jk}(i, j, k = 1, 2)$ are the Cristoffel symbols of the second kind defined as $\Gamma^1_{11} = J^{-1}(x_{\xi\xi}y_\eta - y_{\xi\xi}x_\eta)$, $\Gamma^1_{12} = \Gamma^1_{21} = J^{-1}(x_{\xi\eta}y_\eta - y_{\xi\eta}x_\eta)$, $\Gamma^1_{22} = J^{-1}(x_{\eta\eta}y_\eta - y_{\eta\eta}x_\eta)$, $\Gamma^2_{11} = J^{-1}(-x_{\xi\xi}y_\xi + y_{\xi\xi}x_\xi)$, $\Gamma^2_{12} = \Gamma^2_{21} = J^{-1}(-x_{\xi\eta}y_\xi + y_{\xi\eta}x_\xi)$ and $\Gamma^2_{22} = J^{-1}(-x_{\eta\eta}y_\xi + y_{\eta\eta}x_\xi)$; and subscripts t, ξ, and η indicate differentiation with respect to these variables.

Taking into account the considerations given in section 2, we specify the coastal boundary conditions as

$$\begin{aligned} U &= 0 \quad \text{along constant } \xi \text{ lines} \\ V &= 0 \quad \text{along constant } \eta \text{ lines} \end{aligned} \tag{A4}$$

and the open boundary conditions as

$$\zeta = \zeta^0(\xi, \eta) \cos[\sigma t - \varphi(\xi, \eta)] \quad \text{along constant } \xi \text{ and } \eta \text{ lines} \tag{A5}$$

Here $\zeta^0(\xi, \eta)$ and $\varphi(\xi, \eta)$ are the amplitude and phase lag relative to Greenwich; and σ is the frequency of the tidal wave.

The set of equations (A1) to (A5) is solved on an Arakawa C staggered grid employing a splitting technique and the semi-implicit Crank-Nicolson scheme. As shown by *Androsov et al.* [1995], this scheme is stable if $\Delta t < \max H(|U| + |V|)^{-1}$.

After averaging over a tidal cycle, the tidal energy budget equation in the curvilinear coordinate system, reads,

$$\rho[\langle (JUH(0.5G^2 + g\zeta^2))_\xi \rangle + \langle (JVH(0.5G^2 + g\zeta^2))_\eta \rangle] = -\rho c_D J \langle G^3 \rangle \tag{A6}$$

where the expressions on the left-hand and right-hand sides describe, in terms of the contravariant variables, the divergence of the mean tidal energy flux per unit length and the mean tidal energy dissipation rate, respectively; the angular brackets indicate averaging over a tidal cycle; and the remaining designations are specified above.

Appendix B: A Simple Model Case of Topographic Funneling in Convergent Channels

We consider a simple model case that concerns tidal propagation in a weakly dissipative, narrow channel with small variations in geometry and the topographic length scale being smaller than a characteristic tidal wavelength. The latter of these restrictions is good for the Strait of Gibraltar, while the former concerning small variations in geometry is not. Accordingly, as applied to the strait, the solution given below cannot presume to describe adequately the phenomenon under consideration. Its purpose is solely to illustrate the fact that under some conditions (supercritical convergence and weak friction) typical of the strait, the topographic funnelling effect may, in principle, be responsible for the maintenance of a ~90° phase difference between tidal velocity and elevation that is observable in the strait.

The linearized cross-sectionally integrated equations for conservation of mass and along-channel momentum are

$$b\frac{\partial \zeta}{\partial t} = -\frac{\partial}{\partial x} uA \tag{B1}$$

$$\frac{\partial u}{\partial t} = -g\frac{\partial \zeta}{\partial x} - ru \tag{B2}$$

where u is the along-channel tidal velocity; ζ is the tidal elevation; A and b are the cross-sectional area and the width of a channel, respectively; r is the bottom friction coefficient in the linear resistance law; g is the acceleration due to gravity; x is the along-channel distance; and t is time.

Let u and ζ be time-periodic functions, i.e.,

$$\begin{pmatrix} u \\ \zeta \end{pmatrix} = \mathrm{Re}\begin{pmatrix} \bar{u} \\ \bar{\zeta} \end{pmatrix} \exp(-i\sigma t) \tag{B3}$$

where $\bar{u}$ and $\bar{\zeta}$ are the complex amplitudes of tidal velocity and elevation, and σ is the tidal frequency.

In addition, let A and b be defined as the mean values A_0 and b_0 plus small deviations, the topographic length scale being much less than the characteristic tidal wavelength $(gA_0/b_0)^{1/2}/\sigma$. Then the lowest-order equations (B1) and (B2), in terms of the dimensionless variables $\bar{\zeta}_n = \zeta/\zeta_0$, $\bar{u}_n = \bar{u}/(gb_0/A_0)^{1/2}\zeta_0$ and $x_n = x\sigma(gA_0/b_0)^{-1/2}$ (where ζ_0 is the characteristic tidal elevation), may be reduced to the form

$$\frac{d^2\bar{\zeta}_n}{dx_n^2} + 2\chi\frac{d\bar{\zeta}_n}{dx_n} + (1 + ir/\sigma)\bar{\zeta}_n = 0 \tag{B4}$$

$$\bar{u}_n = -(i + r/\sigma)\frac{d\bar{\zeta}_n}{dx_n} \tag{B5}$$

where $\chi = 0.5(gA_0/\sigma^2 b_0)^{1/2}dA/A_0dx$ is a dimensionless parameter which characterises the convergence rate; and the dimensionless parameter r/σ, defining the friction effect, is considered to be small.

For the sake of simplicity we assume that χ is constant and, following *Jay* (1991), classify the case of $|\chi| = 1$ as the case of critical convergence at which the effects of acceleration and convergence in the wave equation compensate each other. Accordingly, when the acceleration effect exceeds the convergence effect, this situation corresponds to the subcritical convergence ($|\chi| < 1$); otherwise, it corresponds to supercritical convergence ($|\chi| > 1$). For supercritical convergence, which is typical of almost the entire length of the Strait of Gibraltar with χ varying in the range from -10.5 to 18.4, the solution of (B4) and (B5) reads,

$$\begin{aligned}\zeta_n = {} & C_1 \exp\{-[\chi + (\chi^2 - 1)^{1/2}]x_n\} \\ & \cdot \cos\left[t_n - \frac{r/2\sigma}{(\chi^2 - 1)^{1/2}}x_n - \varepsilon_1\right] \\ & + C_2 \exp\{-[\chi - (\chi^2 - 1)^{1/2}]x_n\} \\ & \cdot \cos\left[t_n + \frac{r/2\sigma}{(\chi^2 - 1)^{1/2}}x_n - \varepsilon_2\right]\end{aligned} \tag{B6}$$

$$\begin{aligned}u_n = {} & Y^+C_1 \exp\{-[\chi + (\chi^2 - 1)^{1/2}]x_n\} \\ & \cdot \cos\left[t_n - \frac{r/2\sigma}{(\chi^2 - 1)^{1/2}}x_n - \varepsilon_1 - \theta^+\right] \\ & - Y^-C_2 \exp\{-[\chi - (\chi^2 - 1)^{1/2}]x_n\} \\ & \cdot \cos\left[t_n + \frac{r/2\sigma}{(\chi^2 - 1)^{1/2}}x_n - \varepsilon_2 + \theta^-\right]\end{aligned} \tag{B7}$$

Here the amplitudes Y^+, Y^-, and the phases θ^+, θ^-, of the complex admittances, specifying a transmission of energy, are defined, to the terms of the order r^2/σ^2, as

$$Y^+ = [\chi + (\chi^2 - 1)^{1/2}]$$

$$\theta^+ = \tan^{-1}\frac{(\chi^2 - 1)^{1/2}[\chi + (\chi^2 - 1)^{1/2}]}{(r/2\sigma) + (\chi^2 - 1)^{1/2}[\chi + (\chi^2 - 1)^{1/2}](r/\sigma)}$$

$$Y^- = [\chi - (\chi^2 - 1)^{1/2}]$$

$$\theta^- = \tan^{-1}\frac{(\chi^2 - 1)^{1/2}[\chi - (\chi^2 - 1)^{1/2}]}{(r/2\sigma) - (\chi^2 - 1)^{1/2}[\chi - (\chi^2 - 1)^{1/2}](r/\sigma)}$$

C_1, C_2, and ε_1, ε_2, are coefficients determined from the boundary conditions.

If the channel is short relative to the tidal wavelength, so that the relevant length scale in (B1) and (B2) should be taken as the along-channel dimension, l, and if the latter is much greater than the topographic length scale, then the expressions for the amplitudes and phases of the complex admittances will remain exactly as before. Also, the expressions for tidal elevation and velocity will be formally equivalent to (B6) and (B7) when x_n is replaced by jx_n. Substitution of the definitions $x_n = x/l$ and $j = l(gA_0/\sigma^2 b_0)^{-1/2}$ into jx_n shows that jx_n is nothing more that the dimensionless along-channel distance appearing in the aforementioned equations. Thus, for an arbitrary along-channel scale, the solution of the problem on tidal propagation in channels of convergent/divergent geometry represents two damped progressive waves travelling in the positive and negative x direction. Their decrements are determined by χ and the wavenumbers via a combination of χ and r/σ, so that in the case of weak friction ($r/\sigma \to 0$) the wavenumbers approach zero. This suggests that for supercritical convergence the solution changes its character. That is, progressive waves are transformed into standing waves with a phase difference of about 90° between tidal velocity and elevation. Reflected waves are not therewith excited, as stated by *Jay* [1991] and *Friedrichs and Aubrey* [1994] for exponentially convergent channels, and a substantial transport of energy becomes impossible. The same peculiarities are inherent in critical convergence.

Acknowledgments. This work was carried out during a stay of B. A. Kagan as visiting professor at University of Cadiz. The authors are greatly indebted to A. G. Pufahl and G. A. Kivman for their careful comments and to the reviewers for their constructive criticism of an earlier version of the manuscript. This work was supported by the EC Project SELF-II, contract CT 95-0087, and the INTAS Project 96-1875.

References

Androsov, A. A., K. A. Klevanny, E. S. Salusti, and N. E. Voltzinger, Open boundary conditions for horizontal 2-D curvilinear-grid long-wave dynamics of a strait, *Adv. Water Res.*, *18*, 267–276, 1995.

Candela, J., C. Winant, and A. Ruiz, Tides in the Strait of Gibraltar, *J. Geophys. Res.*, *95*, 7313–7335, 1990.

Defant, A., *Physical Oceanography*, vol. 2, 598 pp., Pergamon, Tarrytown, N. Y., 1961.

Foreman, M. G. G., L. M. Delves, Y. Barrodale, and R. F. Henry, On the use of the Proudman-Heaps tidal theorem, *Geophys. J. R. Astron. Soc.*, *63*, 467–478, 1980.

Friedrichs, C. T., and D. G. Aubrey, Tidal propagation in strongly convergent channels, *J. Geophys. Res.*, *99*, 3321–3336, 1994.

García Lafuente, L. J. M., Variabilidad del nivel del mar en el Estrecho de Gibraltar: Mareas y oscilaciones residuales, Ph.D. thesis, 154 pp., Inst. Esp. de Oceanogr., Fuengirola, Málaga, Spain, 1986.

Hunt, J. N., Tidal oscillations in estuaries, *Geophys. J. R. Astron. Soc.*, *8*, 440–455, 1964.

Jay, D. A., Green's law revisited: Tidal long-wave propagation in channels with strong topography, *J. Geophys. Res.*, *96*, 20,585–20,598, 1991.

Lozano, C. J., and J. Candela, The M_2 tide in the Mediterranean Sea: Dynamical analysis and data assimilation, *Oceanol. Acta*, *18*, 419–441, 1995.

Mañanes, R., M. Bruno, J. Alonso, B. Fraguela, and L. Tejedor, The non-linear interaction between tidal and subinertial barotropic flows in the Strait of Gibraltar, *Oceanol. Acta*, *21*, 33–46, 1998.

McIntosh, P. C., and A. F. Bennett, Open ocean modelling as an inverse problem: M_2 tides in the Bass Strait, *J. Phys. Oceanogr.*, *14*, 601–614, 1984.

Oliger, J., and A. Sandstrom, Theoretical and practical aspects of some

initial boundary-value problems in fluid dynamics, *SIAM J. Appl. Math.*, *35*, 419–446, 1978.

Rocha, C. A., and A. J. Clarke, Interaction of ocean tides through a narrow single strait and narrow multiple straits, *J. Phys. Oceanogr.*, *17*, 2203–2218, 1987.

Ruíz Cañavate, A., Flujos barotrópicos de marea en el Estrecho de Gibraltar, Ph.D. thesis, 123 pp., Univ. de Cádiz, Cádiz, Spain, 1994.

Sánchez, P., and J. R. Pascual, Primeras experiencias en la modelación del Estrecho de Gibraltar, in *Seminario Sobre la Oceanografía Física del Estrecho de Gibraltar*, edited by J. L. Almazán et al., pp. 251–282, Escuela Superior Ing. Caminos, Canales y Puertos, Madrid, 1988.

Tsimplis, M. N., R. Proctor, and R. A. Flather, A two-dimensional tidal model for the Mediterranean Sea, *J. Geophys. Res.*, *100*, 16,223–16,239, 1995.

Wang, D. P., Model of mean and tidal flows in the Strait of Gibraltar, *Deep Sea Res.*, *36*, 1535–1548, 1989.

Wang, D. P., The Strait of Gibraltar model: Internal tide, diurnal inequality and fortnightly modulation, *Deep Sea Res.*, *40*, 1187–1203, 1993.

A. Izquierdo and L. Tejedor, Departamento de Física Aplicada, Universidad de Cádiz, Polígono Río San Pedro, 11519, Puerto Real, Cádiz, Spain. (alfredo.izquierdo@uca.es; luis.tejedor@uca.es)

B. A. Kagan and D. V. Sein, P. P. Shirshov Institute of Oceanology, Russian Academy of Sciences, St. Petersburg Branch, Pervaya Liniya 30, 199053 St. Petersburg, Russia.

(Received August 29, 1996; revised June 30, 1998; accepted September 21, 1998.)